Attenuation and Rotation of Plane-Polarized Ultrasound in Copper in a Longitudinal Magnetic Field*

J. R. Boyd† and J. D. Gavenda
The University of Texas, Austin, Texas
(Received 6 June 1966)

The rotation of the plane of polarization and attenuation of a shear sound wave at 4.2°K have been measured for the propagation vector **q** parallel to the magnetic field **B** in the [001] direction in copper. Frequencies from 30 to 110 Mc/sec were used. Both the attenuation and rotation are periodic in ν/B, where ν is the sound frequency. The period for the attenuation is 0.0201 ± 0.0005 Mc/sec G, whereas the period for the rotation is 0.0402 ± 0.001 Mc/sec G. A theory is presented which describes this effect. The oscillations in the attenuation are of the type predicted by Kaner, Peschanskii, and Privorotskii, with a peak in the attenuation preceding an absorption edge. An absorption edge is observed at about one-fourth the magnetic field value expected for the free-electron case. The results are interpreted in terms of the Fermi surface of copper as put forth by Roaf. A method is suggested for determining $\omega_c\tau$, where ω_c is the cyclotron frequency and τ the relaxation time; a value of $m_c\bar{v}_z=0.381\pm0.009\times10^{-19}$ g cm/sec is assigned to electrons with orbits near the plane $k_z=0.45\times10^8$ cm^{-1}, where m_c is the cyclotron effective mass, $\bar{v}_z$ is the drift velocity, and k_z is the [001] direction.

I. INTRODUCTION

THE literature in recent years has carried the results of many measurements of the attenuation of ultrasound in a metal in a transverse magnetic field. However, very few experimental results have been reported for the longitudinal-field case, i.e., where $\mathbf{B}\|\mathbf{q}$ ($\mathbf{q}$ is the propagation vector of the sound wave). The theory of ultrasonic attenuation in pure metals at low temperatures for shear waves propagating parallel to an external magnetic field has been worked out by a number of authors.[1–3]

These authors consider a circularly polarized shear sound wave propagating in a metal single crystal. The external magnetic field **B** and the propagation vector **q** are taken along the z axis of a coordinate system. Thus the lattice displacement **s**, the lattice velocity $\mathbf{u}=\partial\mathbf{s}/\partial t$, and the resulting internal electric field **E** are all perpendicular to **B**. These conditions are those which characterize a cyclotron resonance experiment except that the frequency ω of the sound wave (and hence of the electric field **E**) is lower by a factor of about 10^3 than the frequencies employed in such experiments. However, as an electron executes an orbit on the Fermi surface in a plane perpendicular to **B** it also drifts along the axis with a velocity $\bar{v}_z$ which is the average z component of its Fermi velocity. Therefore the electron does not see a sound wave of frequency ω, but rather a Doppler-shifted or "effective" frequency ω_e given by

$$\omega_e=\omega(\bar{v}_z/c_s-1), \tag{1}$$

where c_s is the velocity of sound in the sample.

It is possible for an electron to gain energy from the sound wave via interaction with the accompanying electric field (we neglect the deformation potential contributions here) if the electron stays in phase with the sound field, and if its mean free path l is long enough so that it may sample the electric field over a distance of the order of a wavelength of sound before it is scattered. Such a condition of constant phase will be met by an electron which executes one cyclotron orbit around the Fermi surface while traveling in the z direction a distance equal to one wavelength of sound. This amounts to setting $\omega_c=\omega_e$:

$$\omega_c=\omega(\bar{v}_z/c_s-1), \tag{2}$$

where $\omega_c=eB/m_cc$ is the cyclotron frequency and m_c is the cyclotron mass of the electron. (Since $\bar{v}_z/c_s\gg1$ for most electrons, the 1 will be neglected in most of the discussion that follows.)

It can be seen that, for values of **B** such that $\omega_c<\omega\bar{v}_z^{\max}/c_s$, there will be a group of electrons on the Fermi surface with the correct value of $\bar{v}_z$ to satisfy Eq. (2) and that these electrons will gain energy from the sound wave, thus giving rise to attenuation. It is possible of course that the magnetic field may be so large that Eq. (2) cannot be satisfied by even the maximum value of $\bar{v}_z$. In this case the attenuation falls off to zero and one observes the absorption edge first predicted by Kjeldaas.[1]

Circularly polarized sound waves are difficult to generate, but one may perform the experiment with plane-polarized shear waves, making use of the fact that such waves can be resolved into right- and left-circularly polarized waves of equal amplitudes. As these two waves propagate through the metal they suffer different velocity changes and hence acquire a phase difference.

* This work was supported by the National Science Foundation and the U. S. Office of Naval Research and is based on a dissertation by J. R. Boyd submitted to the University of Texas in partial fulfillment of the requirements for the degree of Doctor of Philosophy.

† Present address: Center for the Study of Materials, Case Institute of Technology, Cleveland, Ohio.

[1] T. Kjeldaas, Jr., Phys. Rev. **113**, 1473 (1959).

[2] G. L. Kotkin, Zh. Eksperim. i Teor. Fiz. **41**, 281 (1961) [English transl.: Soviet Phys.—JETP **14**, 201 (1962)].

[3] M. H. Cohen, M. J. Harrison, and W. A. Harrison, Phys. Rev. **117**, 937 (1960).

This causes the plane of polarization of the sound wave to rotate by one half the phase difference of the right- and left-circularly polarized waves. Since the receiving transducer is sensitive only to the component of particle motion in a particular direction, this rotation results in an "apparent" attenuation added to the true attenuation of the wave.

The rotation of the plane of polarization has been studied by Kjeldaas[1] in terms of the magnetoconductivity tensor, and by Kotkin[2] and Vlasov and Filippov,[4] who relate it to the dynamic elastic constants of the metal.

There are few published papers dealing with the experimental observation of these effects. Mackintosh[5] has measured the attenuation of plane-polarized shear waves in tin and Jones[6] has reported similar measurements in aluminum. Although both of these papers report the observation of absorption edges in the attenuation as a function of the magnetic field, neither took into account the rotation of the plane of polarization which, according to Kjeldaas,[1] should be greatest at the absorption edge. Miller[7] has measured the attenuation of circularly polarized sound waves in tin.

The purpose of this investigation is to measure the rotation of the plane of polarization of a shear sound wave in copper as a function of magnetic field intensity and sound frequency and to determine the true attenuation curve by correcting for the effects caused by the rotation. The results are interpreted in a simple geometric manner in terms of the expression for the Fermi surface of copper as put forth by Roaf.[8]

In Sec. II the theoretical ideas are reviewed. In Secs. III and IV the experimental arrangement and method of data analysis are given. Section V presents the experimental results and Sec. VI deals with the interpretation of the results.

A preliminary report of the results of this work has already been published.[9]

II. THEORY

Most of the theoretical work on this problem has assumed the validity of the free-electron theory of metals. The work of Kotkin[2] does not contain this assumption, but he does assume an infinite electron mean free path. The results of the free-electron theory will be quoted here and then we shall consider the effects that arise from a nonspherical Fermi surface.

We consider a transverse sound wave propagating through a metal single crystal in a direction of cubic symmetry and parallel to an external magnetic field $\mathbf{B}$. Vlasov and Filippov[4] have shown that, for such a situation, the normal modes are circularly polarized. The direction of propagation is taken along the z axis. The space and time variation of the sound wave is assumed to be given by $\exp[i(qz-\omega t)]$. It follows then that all quantities which depend on the sound field, such as the particle velocity $\mathbf{u}$ and the electric field $\mathbf{E}$, have the same space and time dependence; therefore one may write $\partial/\partial z=iq$ and $\partial/\partial t=-i\omega$.

As a starting point one writes down the Boltzmann transport equation for the electron distribution function, Maxwell's equations for the internal electric and magnetic fields $\mathbf{E}$ and $\mathbf{b}$ that are set up by the sound wave, and the equation of motion of the lattice for a circularly polarized sound wave. The self-consistent solution of these equations allows one to find the attenuation and dispersion of the sound wave.

The Boltzmann equation is

$$\partial f/\partial t+\mathbf{v}\cdot(\partial f/\partial \mathbf{r})+\dot{\mathbf{k}}\cdot(\partial f/\partial \mathbf{k})=(\partial f/\partial t)_{\text{coll}}, \quad (3)$$

where $f(\mathbf{r},\mathbf{k},t)$ is the distribution function of the electrons.

A relaxation time τ is introduced in the standard manner:

$$(\partial f/\partial t)_{\text{coll}}=-[f(\mathbf{r},\mathbf{k},t)-f_0(\mathbf{r},\mathbf{k}-m\mathbf{u}/\hbar,t)]/\tau(\mathbf{k}). \quad (4)$$

The function $f_0(\mathbf{r},\mathbf{k}-m\mathbf{u}/\hbar,t)$ is a Fermi distribution function shifted in $\mathbf{k}$ space by $m\mathbf{u}/\hbar$. This takes into account the effect of collision drag as developed by Holstein.[10] The solution to the Boltzmann equation is

$$\eta(k_z,\phi)=\int_{-\infty}^{\phi}\frac{\Gamma(k_z,\phi')}{\omega_c(k_z)}\exp\left[\int_{\phi}^{\phi'}\frac{1+i\omega_c\tau}{\omega_c\tau}d\phi''\right]d\phi', \quad (5)$$

where

$$\Gamma(\mathbf{k})=-e\mathbf{v}\cdot(\mathbf{E}-m\mathbf{u}/e\tau)\equiv-e\mathbf{v}\cdot\mathbf{D} \quad (6)$$

and

$$f(\mathbf{r},\mathbf{k},t)=f_0-\eta(\mathbf{r},\mathbf{k},t)(\partial f_0/\partial\epsilon).$$

One may calculate the electronic current as follows:

$$\mathbf{j}=(e/4\pi^3)\int\mathbf{v}\eta(\partial f_0/\partial\epsilon)d\mathbf{k}. \quad (7)$$

We now use Maxwell's equations to eliminate $\mathbf{j}$:

$$\nabla\times\mathbf{b}=(4\pi/c)(\mathbf{j}+\mathbf{J}), \quad c\nabla\times\mathbf{E}=-\partial\mathbf{b}/\partial t, \quad (8)$$

where $\mathbf{J}$ is the lattice current and $\mathbf{b}$ is the magnetic field set up by the sound wave. Finally we proceed to the equation of motion of the lattice:

$$\partial^2\mathbf{s}/\partial t^2=c_0^2\partial^2\mathbf{s}/\partial z^2+\mathbf{F}_d, \quad (9)$$

where $\mathbf{F}_d$ is the force per unit mass acting on the ions and c_0 is the sound velocity in the absence of any perturbations. There are two such forces, the Lorentz

[4] K. B. Vlasov and B. N. Filippov, Zh. Eksperim. i Teor. Fiz. 44, 922 (1963) [English transl.: Soviet Phys.—JETP 17, 628 (1963)].
[5] A. R. Mackintosh, Phys. Rev. 131, 2420 (1963).
[6] B. K. Jones, Phil. Mag. 9, 217 (1964).
[7] B. I. Miller, Bull. Am. Phys. Soc. 10, 371 (1965).
[8] D. J. Roaf, Phil. Trans. Roy. Soc. London A255, 135 (1962).
[9] J. D. Gavenda and J. R. Boyd, Phys. Rev. Letters 15, 364 (1965).
[10] T. Holstein, Phys. Rev. 113, 479 (1959).

force on the ions and a collision force:

$$\mathbf{F}_d=(e/M)[\mathbf{E}+(\mathbf{u}\times\mathbf{B})/c]+(m/M)(\langle\mathbf{v}\rangle-\mathbf{u})/\tau, \quad (10)$$

where M is the mass of an ion.

The self-consistent solution of Eqs. (7), (8), and (9) leads to the following equation (after converting to circularly polarized components $E^{\pm}=E_x\pm iE_y$, etc.):

$$\left[\omega^2-c_0^2q^2\pm\Omega_c\omega-\frac{im\omega}{M\tau}\frac{(1+i\beta)(1-G^{\pm})}{(G^{\pm}+i\beta)}\right]s^{\pm}=0, \quad (11)$$

where $\Omega_c=eB/Mc$ is the ion cyclotron frequency $\beta=(c/c_s)^2(\omega/4\pi\sigma_0)$, and

$$G^{\pm}=3/4\int_0^{\pi}\frac{\sin^3\theta d\theta}{1-i\tau(\omega\pm\omega_c-qv_0\cos\theta)} \quad (12)$$

for a free-electron Fermi surface.

Equation (11) or its equivalent was derived by Kjeldaas,[1] Quinn and Rodriguez,[11] and Langenberg and Bok,[12] although Langenberg and Bok neglected the Lorentz force on the ions and Kjeldaas neglected the collision force on the lattice. The complete solution of Eq. (11), as pointed out by Quinn and Rodriguez,[11] yields right- and left-circularly polarized acoustic waves and a left-circularly polarized electromagnetic wave called a helicon. The properties of helicons and their interaction with acoustic waves are discussed by Quinn and Rodriguez[11] and by Kaner and Skobov.[13–15]

Below the Kjeldaas edge, that is, for $\omega_c<q\bar{v}_z^{(\max)}$, the helicon waves are damped out. Above the edge, the normal modes of the system are circularly polarized acoustic waves and a helicon wave, and as such they are only weakly coupled except near resonance, where their wavelengths coincide. At this helicon-phonon crossover, the sound wave undergoes a resonant attenuation and generates a helicon wave. However, for the acoustic frequencies and magnetic fields used in this experiment we need not concern ourselves with the helicon solution. For copper, assuming free-electron values of the parameters, the helicon-phonon interaction takes place at magnetic fields of the order of 10^8 G. We may neglect β at the frequencies and magnetic fields used here ($B\approx10^4$ G, $\omega\approx10^8$ sec^{-1}) because $\beta\simeq10^{-4}$ while $|G^{\pm}|\simeq10^{-1}$. If we let $\omega^{\pm}=\omega_1^{\pm}+i\omega_2^{\pm}$, where $\omega_1^{\pm}$ and $\omega_2^{\pm}$ are real, we have

$$\omega_1^{\pm}=c_0q\mp\Omega_c/2+(m/2M\tau)\,\mathrm{Im}(1/G^{\pm}-1), \quad (13)$$

and

$$\omega_2^{\pm}=(m/2M\tau)\,\mathrm{Re}(1/G^{\pm}-1). \quad (14)$$

Here the dependence of $G^{\pm}$ on ω has been ignored. One should carry out a self-consistent solution of (11) and (12). It can be seen that the effect of the external magnetic field is to split the frequency degeneracy of the two circularly polarized sound waves.

The energy attenuation per cm $A^{\pm}$ is given by

$$A^{\pm}=(m/M\tau c_0)\,\mathrm{Re}(1/G^{\pm}-1). \quad (15)$$

The velocity of sound is given by

$$c_s^{\pm}=c_0[1\mp\Omega_c/2\omega+(m/2M\omega\tau)\,\mathrm{Im}(1/G^{\pm})]. \quad (16)$$

Figure 1 shows a plot of A^+ versus γ^+ (proportional to B) given by Kjeldaas.[1] The absorption edge can be seen at $\gamma^+=1$.

The preceding paragraphs present the main ideas in the theory of the attenuation and dispersion of a circularly polarized sound wave propagating parallel to **B** in an ideal metal. The physical picture is that, as the magnetic field is increased from zero, the band of electrons contributing to the attenuation leaves the central cross section of the Fermi surface and "slides out" on the surface in the direction of **B**. This may be seen by a consideration of the expression for $G^{\pm}$ given in Eq. (12), which may be rewritten as follows:

$$G^{\pm}=\frac{3}{4}\int_0^{\pi}\frac{\sin^3\theta[1+i\tau(\omega\pm\omega_c-qv_0\cos\theta)]d\theta}{1+\tau^2(\omega\pm\omega_c-qv_0\cos\theta)^2}. \quad (17)$$

The real part of the integrand has a peak at $\omega\pm\omega_c-qv_0\cos\theta=0$ and falls off to zero at a rate dependent on the value of ql, the width of the peak being proportional to $(ql)^{-1}$. Thus only bands of electrons which satisfy

$$qv_0\cos\theta=\omega\pm\omega_c \quad (18)$$

contribute to $G^{\pm}$ and hence to the attenuation. This, however, is just the condition set forth in Eq. (2), except that it takes into account both polarizations. We see that for the (+) sign in Eq. (18), $\cos\theta=(\omega+\omega_c)/qv_0$, whereas for the (−) sign $\cos\theta=(\omega-\omega_c)/qv_0$. Since $\omega_c\gg\omega$ this means that the band of electrons on one side of the Fermi surface interacting with the (+) wave

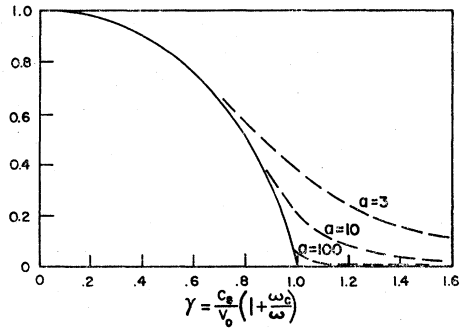

FIG. 1. Attenuation of a right-circularly polarized acoustic wave in a free-electron metal versus γ. γ is approximately proportional to the magnetic field. The curves for the different $a=ql$ are normalized to 1 at $\gamma=0$ (after Kjeldaas, Ref. 1).

[11] J. J. Quinn and S. Rodriguez, Phys. Rev. **133**, A1589 (1964).
[12] D. N. Langenberg and J. Bok, Phys. Rev. Letters **11**, 549 (1963).
[13] E. A. Kaner and V. G. Skobov, Zh. Eksperim. i Teor. Fiz. **45**, 610 (1963) [English transl.: Soviet Phys.—JETP **18**, 419 (1963)].
[14] V. G. Skobov and E. A. Kaner, Zh. Eksperim. i Teor. Fiz. **46**, 273 (1964) [English transl.: Soviet Phys.—JETP **19**, 189 (1964)].
[15] E. A. Kaner and V. G. Skobov, Zh. Eksperim. i Teor. Fiz. **46**, 1106 (1964) [English transl.: Soviet Phys.—JETP **19**, 749 (1964)].

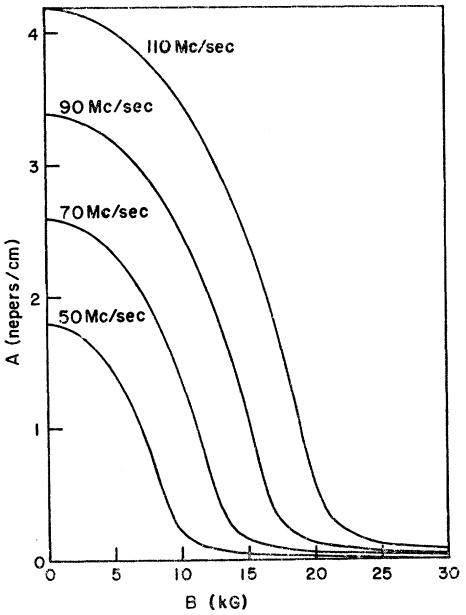

FIG. 2. Attenuation of a shear wave versus magnetic field for several frequencies in free-electron copper. ql is taken to be 10 at 50 Mc/sec.

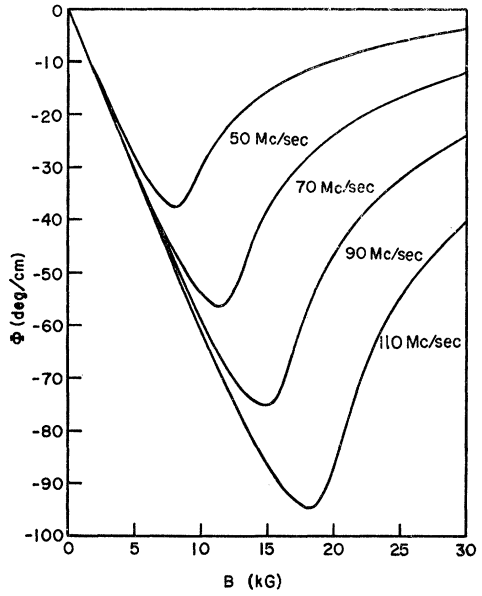

FIG. 3. Rotation of the plane of polarization of a shear wave versus magnetic field for several frequencies in free-electron copper. ql is taken to be 10 at 50 Mc/sec.

differs slightly from the mirror image of the band of electrons on the other side of the Fermi surface interacting with the (−) wave, therefore in general $A^+\neq A^-$ and $c_s^+\neq c_s^-$. If one is using plane-polarized sound waves, this will lead to the appearance of a rotation of the plane of polarization and an ellipticity of the wave. The effects of the ellipticity will be discussed later.

The attenuation per cm of a (rotating) plane wave is given by

$$A=(m/2M\tau c_0)[\mathrm{Re}(1/G^+)+\mathrm{Re}(1/G^-)-2], \quad (19)$$

and the rotation of the plane of polarization in radians per cm of path is given by one half the phase difference between the two circularly polarized waves:

$$\Phi=(\Omega_c/2c_0)\{1+[\mathrm{Im}(1/G^-)-\mathrm{Im}(1/G^+)]/2\omega_c\tau\}. \quad (20)$$

This equation displays the fact that the rotation should be considered as the result of moving the ions in a magnetic field, but with the ion charge modified by a "screening" factor given by the second term in the braces. We also note that since $G^-(\mathbf{B})=G^+(-\mathbf{B})$ and $\Omega_c(-\mathbf{B})=-\Omega_c(\mathbf{B})$, we have $A(\mathbf{B})=A(-\mathbf{B})$ and $\Phi(\mathbf{B})=-\Phi(-\mathbf{B})$.

Figure 2 shows a plot of Eq. (19) for several frequencies, using parameters representative of our copper sample. The absorption edge is seen to be rather diffuse for our experimental conditions. Figure 3 shows a plot of Eq. (20) for the same parameters. It is seen that even for the free-electron case the rotation is considerable.

If one considers a "real-metal" (nonspherical) Fermi surface, the development presented for the spherical surface is inadequate. It has been shown by Pippard,[16] Kaner, Peschanskii, and Privorotskii,[17] and Stolz[18] that one must take into account the deformation of the surface by a lattice strain by means of a "deformation potential." Stolz finds (Eq. IV.28, Ref. 18) the following expression for the attenuation:

$$A=A_0\,\mathrm{Re}\int(m_c/\omega_c)\int_0^{2\pi}G_A^*(\phi,k_z)\int_{-\infty}^{\phi}G_A(\phi',k_z)$$

$$\times\exp\left\{\int_{\phi}^{\phi'}[(1+i\omega_c\tau)/\omega_c\tau]d\phi''\right\}d\phi d\phi' dk_z, \quad (21)$$

where

$$A_0=(4\pi^3\hbar^2\rho c_0u^2)^{-1},$$

ρ is the density of the metal, and G_A is the electron-phonon interaction parameter. The rest of the symbols have already been defined. G_A includes the interaction due to the electric field, collision drag, and the deformation terms (see Eq. II.30A of Ref. 18, for example). The exact calculation of some of the terms in G_A becomes quite difficult even if an expression for the Fermi surface is known. However, for the following arguments we need not concern ourselves with the detailed form of G_A.

If we modify Eq. (21) for (±) circularly polarized

[16] A. B. Pippard, Proc. Roy. Soc. (London) **A257**, 165 (1960).
[17] E. A. Kaner, V. G. Peschanskii, and I. A. Privorotskii, Zh. Eksperim. i Teor. Fiz. **40**, 214 (1961) [English transl.: Soviet Phys.—JETP **13**, 147 (1961)].
[18] H. Stolz, Phys. Status Solidi **3**, 1153 (1963).

waves and let $\mathbf{q}\cdot\mathbf{v}-\omega=qv_z-q\bar{v}_z+\omega_e$ we get

$$A^{\pm}=A_0\,\mathrm{Re}\int(m_c/\omega_c)\int_0^{2\pi}G_A^{\pm*}(\phi,k_z)\int_{-\infty}^{\phi}G_A^{\pm}(\phi',k_z)\times\exp\left\{\int_{\phi}^{\phi'}[i(qv_z-q\bar{v}_z)/\omega_c-(1+i\omega_e\tau)/\omega_c\tau]d\phi''\right\}\times d\phi d\phi' dk_z. \quad (22)$$

Now $qv_z-q\bar{v}_z$ and $G_A(\phi,k_z)$ possess the symmetry of the Fermi surface which is fourfold for the [001] direction in copper, therefore we may make the following expansion:

$$G_A^{\pm}(\phi,k_z)\exp\left\{i\int_0^{\phi}[(qv_z-q\bar{v}_z)/\omega_c]d\phi''\right\}=\sum_{n=-\infty}^{\infty}a_n^{\pm}(k_z)e^{i(4n\pm1)\phi}. \quad (23)$$

Thus we find

$$A^{\pm}=A_0\,\mathrm{Re}\int(m_c/\omega_c)\times\sum_{n,\nu=-\infty}^{\infty}a_n^{\pm}a_\nu^{\pm*}\int_0^{2\pi}\int_{-\infty}^{\phi}\exp\left\{i(4n\pm1)\phi'-i(4\nu\pm1)\phi+\int_{\phi}^{\phi'}[(1+i\omega_e\tau)/(\omega_c\tau)]d\phi''\right\}d\phi d\phi' dk_z. \quad (24)$$

Integrating over ϕ'', ϕ', and ϕ we arrive at

$$A^{\pm}=2\pi A_0\,\mathrm{Re}\sum_{n=-\infty}^{\infty}\int\frac{m_c\tau|a_n^{\pm}(k_z)|^2dk_z}{1+i\tau[\omega_e+(4n\pm1)\omega_c]}, \quad (25)$$

where we have used the relationship

$$\int_0^{2\pi}\exp\{i4(n-\nu)\phi\}d\phi=2\pi\delta_{n,\nu}.$$

Equation (25) is equivalent to Stolz's Eq. (VII.22), but modified for a fourfold symmetric surface and for circularly polarized sound waves.

The main contribution to the above integral will occur for $\omega_e=q\bar{v}_z-\omega=-(4n\pm1)\omega_c$. In most cases of interest $\omega\ll\omega_c$ so this condition may be written as

$$q\bar{v}_z/\omega_c=-(4n\pm1),\quad(n=0,\pm1,\pm2,\cdots). \quad (26)$$

From Eq. (26) we see that the attenuation is quasi-periodic in $q\bar{v}_z/\omega_c$. We shall assume here that the variation of the numerator in Eq. (25) is sufficiently slow so that it does not drastically alter the form of the result. It will be shown that the main features of the experimental curves may be understood by consideration of the resonant denominators in Eq. (25).

As each of the contributing bands of electrons slides out on the Fermi surface with increasing magnetic field, it gives rise to a sudden decrease in the attenuation such as those discussed by Gurevich.[19] These decrements are smooth if $(q\bar{v}_z/\omega_c)_{\max}$ occurs at $k_z=k_z^{\max}$, that is, if the band of electrons contributing to the attenuation approaches the limiting point of the Fermi surface in the direction of $\mathbf{B}$ as B increases. However, Kaner, Peschanskii, and Privorotskii[17] and Stolz[18,20] have shown that if $(q\bar{v}_z/\omega_c)_{\max}$ occurs at $k_z<k_z^{\max}$, there are peaks in the attenuation. In this situation the bands of electrons satisfying Eq. (26) approach some plane on the Fermi surface between the central orbit at $k_z=0$ and the limiting point at $k_z^{\max}$ as the magnetic field increases. As we shall see later, one expects copper to display these peaks in attenuation.

It should be noted here that, while the collision drag and deformation terms are expected to yield slowly varying $a_n^{\pm}(k_z)$ in the numerator of Eq. (25), such is not the case for the electric field term. The self-consistent electric field can be expressed in terms of an effective conductivity which can be expanded in a form similar to Eq. (25). However, for a constant-current system it is the inverse of the conductivity which enters into G_A, so antiresonances as well as resonances are possible when Eq. (26) is satisfied. The fact that our measurements in copper show resonances rather than antiresonances indicates the deformation term dominates the attenuation in regions of the Fermi surface where $(q\bar{v}_z/\omega_c)$ has a maximum, a not entirely unexpected result.

Similarly it can be shown that the change in the sound velocity with field is given by

$$\Delta c_s^{\pm}=C_0\,\mathrm{Im}\sum_{n=-\infty}^{\infty}\int\frac{m_c\tau|a_n^{\pm}(k_z)|^2dk_z}{1+i\tau[\omega_e+(4n\pm1)\omega_c]}, \quad (27)$$

where C_0 includes various constants which are not of interest here. Here we ignore the contribution of the Lorentz force on the ions since it will be linear in B and our present concern is primarily with resonance effects. Therefore we may write

$$A\propto R^{+}+R^{-} \quad (28)$$

and

$$\Phi\propto I^{-}-I^{+}, \quad (29)$$

where

$$R^{\pm}\equiv\sum_{n=-\infty}^{\infty}\int\frac{m_c\tau|a_n^{\pm}|^2dk_z}{1+\tau^2[\omega_e+(4n\pm1)\omega_c]^2} \quad (30)$$

and

$$I^{\pm}\equiv-\sum_{n=-\infty}^{\infty}\int\frac{m_c\tau^2|a_n^{\pm}|^2[\omega_e+(4n\pm1)\omega_c]dk_z}{1+\tau^2[\omega_e+(4n\pm1)\omega_c]^2}. \quad (31)$$

[19] V. L. Gurevich, Zh. Eksperim. i Teor. Fiz. **37**, 71 (1959) [English transl.: Soviet Phys.—JETP **10**, 51 (1960)].
[20] H. Stolz, Phys. Status Solidi **3**, 1493 (1963).

Using $|a_{-n}^{\pm}|^2=|a_n^{\pm}|^2$ we find

$$R^{\pm}=\sum_{n=0}{}'\int m_c\tau|a_n^{\pm}|^2\left\{\frac{1}{1+\tau^2[\omega_c+(4n\pm1)\omega_c]^2}+\frac{1}{1+\tau^2[\omega_c-(4n\mp1)\omega_c]^2}\right\}dk_z, \quad (32)$$

where the prime on the summation sign means that the term for $n=0$ must be multiplied by one-half. One obtains resonances for either the positive or the negative values of $\bar{v}_z$ from alternate terms in the series for the (+) and (−) waves, respectively. Using the symmetry of the Fermi surface about the plane $k_z=0$ we find that $v(k_z)=-v(-k_z)$, $\omega_c(k_z)=\omega_c(-k_z)$, and $|a_n^{\pm}(k_z)|=|a_n^{\pm}(-k_z)|\equiv|a_n|$. If we assume that $\omega\ll\omega_c$ so that $\omega_e\cong q\bar{v}_z$, it follows that $R^+=R^-\equiv R$, and the sum can be rewritten as

$$R=\sum_{n=0}^{\infty}\int_{-k_z\max}^{k_z\max}\frac{m_c\tau|a_n|^2dk_z}{1+\tau^2[q\bar{v}_z-(2n+1)\omega_c]^2}. \quad (33)$$

In a similar fashion we find that

$$I^+=-I^-=\sum_{n=0}^{\infty}(-1)^n\times\int_{-k_z\max}^{k_z\max}\frac{m_c\tau^2|a_n|^2[q\bar{v}_z-(2n+1)\omega_c]dk_z}{1+\tau^2[q\bar{v}_z-(2n+1)\omega_c]^2}. \quad (34)$$

We note that the shifts in velocity will have opposite signs for the two different circularly polarized waves, and furthermore, that the signs will reverse for successive resonances.

We can obtain the qualitative behavior of the attenuation and rotation by assuming that the integrands are dominated by the resonant denominators and considering the remaining terms to be slowly varying. The resonances occur for $|q\bar{v}_z/\omega_c|=2n+1$. For a given B, q, and n, the group of electrons with the appropriate value of $q\bar{v}_z/\omega_c$ to satisfy this condition will dominate the attenuation, but the range of integration over k_z for which this contribution is made will depend on the slope of $q\bar{v}_z/\omega_c$. If $d(q\bar{v}_z/\omega_c)/dk_z\equiv(q\bar{v}_z/\omega_c)'$ is large, the range will be small; if $(q\bar{v}_z/\omega_c)'$ is small the range will be large, thus giving a larger contribution. Therefore, peaks in the attenuation should occur for those field values for which the contributing band of electrons has a minimum in $(q\bar{v}_z/\omega_c)'$. This is the physical argument for the attenuation peaks first described by Kaner, Peschanskii, and Privorotskii.[17] In their paper and also in one by Stolz[20] the mathematical basis for the peaks is presented. The mathematical arguments are given in Appendix A. The results are

$$R=2\pi\xi|b|^{-1}m_c\tau\sum_{n=0}^{\infty}|a_n|^2M_1(b,\xi,\mu_n) \quad (35)$$

and

$$I^{\pm}=\pm2\pi\xi|b|^{-1/2}m_c\tau\sum_{n=0}^{\infty}(-1)^n|a_n|^2M_2(b,\xi,\mu_n), \quad (36)$$

where

$$\xi=(\omega_c\tau)^{-1},\ \mu_n=|(q\bar{v}_z/\omega_c)_{k_1}|-(2n+1),\ b=(q\bar{v}_z/\omega_c)''_{k_1},$$

k_1 is the value of k_z where $(q\bar{v}_z/\omega_c)'=0$, and M_1 and M_2 are defined in (A2) and (A3). Figure 4 shows the behavior of M_1 and M_2 near a resonance. We shall see in Sec. VI that $b<0$ for electrons which cause the resonances in copper. For $b<0$, $M_1(b,\xi,\mu_n)$ has a peak at

$$\mu_n=\Delta_0 \quad (37)$$

and $M_2(b,\xi,\mu_n)$ has a peak at

$$\mu_n=-\Delta_0, \quad (38)$$

where $\Delta_0=3^{-1/2}(\omega_{c0}\tau)^{-1}$ and ω_{c0} is the cyclotron frequency for the condition $q\bar{v}_z/\omega_c=1$.

Thus we see that the attenuation A is described by a series of peaks of the type shown for $M_1(b,\xi,\mu_n)$ in Fig. 4, the selection rule for the peaks being

$$|q\bar{v}_z/\omega_c|=(2n+1)+\Delta_0. \quad (39)$$

The arguments for the rotation curves are similar but with two important differences. First, the selection rule for the peaks is

$$|q\bar{v}_z/\omega_c|=(2n+1)-\Delta_0. \quad (40)$$

This means that the attenuation peaks and rotation peaks are shifted from the condition $|q\bar{v}_z/\omega_c|=(2n+1)$ by an amount $\pm\Delta_0$, respectively. A measurement of this shift would determine $\omega_{c0}\tau$. The second point to be observed is that consideration of Eqs. (29) and (34) shows that the resonances in Φ caused by the odd values

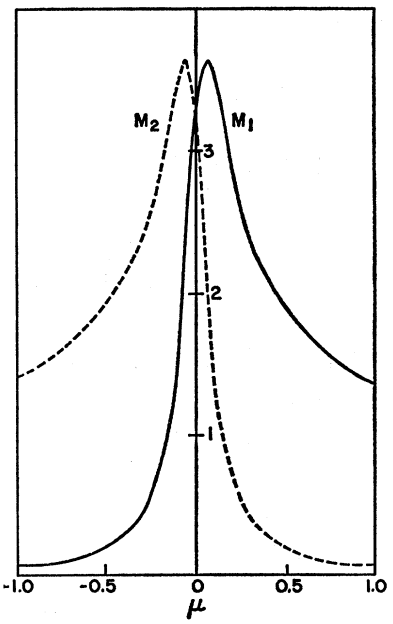

FIG. 4. Resonance functions $M_1(b,\xi,\mu)$ (solid line) and $M_2(b,\xi,\mu)$ (dashed line) versus μ for $b<0$ and $\xi=0.1$.

of n are positive maxima while those caused by the even values of n are negative maxima. This causes the period of oscillation in the Φ curves to be twice that of the A curves. This effect has been observed in the present work.

The attenuation, rotation of the plane of polarization, and ellipticity of the sound wave can be put in terms of the elastic constants of the metal. For $\mathbf{B}\|\mathbf{q}$ along a crystallographic axis Vlasov and Fillipov[4] have shown that

$$(\omega^{\pm})^2=(C_{44}\mp iC_{45})q^2/\rho\,, \tag{41}$$

where C_{44} and C_{45} are elastic constants and ρ is the density of the metal. From this equation we see that right- and left-circularly polarized waves propagate differently in the metal in a magnetic field. The metal is no longer isotropic. The appearance of the rotation and ellipticity of an initially plane-polarized wave is caused by this anisotropy. From an experimental point of view this equation points out a difficulty: Additional rotation and ellipticity will be generated when the wave goes from an isotropic medium (the bond material between the transducer and the sample) to the anisotropic metal. These effects will depend on the bond thickness. In principle they could be eliminated by the use of a quarter-wavelength bond, but experimentally this is a problem.

It is also shown in Ref. 4 that

$$A=(q\ \mathrm{Im}C_{44})/(2\ \mathrm{Re}C_{44})\,, \tag{42}$$

$$\Phi=(q\ \mathrm{Im}C_{45})/(2\ \mathrm{Re}C_{44})\,, \tag{43}$$

and

$$\epsilon=\tanh[(q\ \mathrm{Re}C_{45})/(2\ \mathrm{Re}C_{44})]\,, \tag{44}$$

where ϵ is the ellipticity, i.e., the axial ratio, of the elliptically polarized wave.

III. EXPERIMENTAL PROCEDURE

The measurements were carried out at 4.2°K using a single crystal grown from 99.999% pure copper. At 4.2°K the electron mean free path was impurity-limited.

The sound wave was generated by electrically exciting a quartz transducer with a fundamental resonance at 10 Mc/sec with the output of a pulsed oscillator. The transducers were bonded to the sample with Nonaq stopcock grease. Frequencies from 30 to 110 Mc/sec were employed. The signal from the receiving transducer was amplified, detected, and displayed on an oscilloscope. A gating circuit selected the proper signal echo and fed it into an integrator and logarithmic amplifier. The output of the logarithmic amplifier, which is proportional to the attenuation, was connected to the Y axis of an X-Y recorder. The X axis was connected to the output of a rotating-coil fluxmeter which sampled the magnetic field. Magnetic fields up to 10^4 G were produced by a 7-in. Harvey-Wells electromagnet having poles tapered to a diameter of four inches. The attenuation and magnetic field values were also punched on paper tape for later analysis on a CDC 1604 computer. The attenuation values were calibrated relative to the $B=0$ value by a voltage measurement. Magnetic field values were calibrated with NMR equipment.

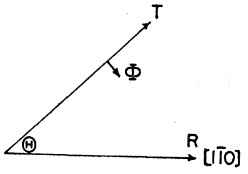

FIG. 5. Schematic of the relative orientations of planes of polarization of the transmitting (T) and receiving (R) transducers on the (001) faces of the sample. The angle of rotation of the transmitted wave is indicated by Φ.

The ac-cut transducers produce a shear sound wave whose plane of polarization is known. The arrangement of the direction of the planes of polarization of the transducers is shown schematically in Fig. 5. On one (001) face of the sample the receiving transducer R is oriented so that its plane of polarization lies along the [1$\bar{1}$0] crystal direction. On the other end of the sample, the plane of polarization of the transmitting transducer T makes an angle θ with R.

The experiments consisted of measuring the attenuation $\alpha(\mathbf{B})$, then reversing the magnetic field and measuring $\alpha(-\mathbf{B})$. These two curves are different because the rotation is reversed when the magnetic field is reversed, and allow one to separate the effect of the actual attenuation $A(\mathbf{B})$ from the effect of the rotation of the plane of polarization $\Phi(\mathbf{B})$ as is shown in the next section.

It is also possible to use two receiving transducers whose planes of polarization are rotated 90° from each other. One may measure the attenuation using each transducer without reversing the field. However, this introduces one more transducer bond and it is then necessary, in the analysis of the data, to add two curves taken with different bonds.

IV. DATA ANALYSIS

If we assume that positive rotation is toward R, then we see from Fig. 5 that

$$\begin{aligned}\alpha(\mathbf{B})L&=-\ln\{|\cos[\theta-\Phi(B)L]|\,|\cos\theta|^{-1}e^{-A(B)L}\},\\ \alpha(-\mathbf{B})L&=-\ln\{|\cos[\theta+\Phi(B)L]|\,|\cos\theta|^{-1}e^{-A(B)L}\},\end{aligned} \tag{45}$$

where we have used $A(\mathbf{B})=A(-\mathbf{B})$ and $\Phi(-\mathbf{B})=-\Phi(\mathbf{B})$. L is the path length, α is the measured attenuation in Np/cm, A is the actual attenuation in Np/cm, and Φ is the rotation in rad/cm.

In deriving Eq. (45) we have neglected the effect of the ellipticity. This should be serious only when the plane of polarization has rotated to approximately 90° from the sensitive direction of the receiving transducer.

Subtracting one equation from the other we obtain

$$\begin{aligned}&[\alpha(-\mathbf{B})-\alpha(\mathbf{B})]L\\ &\quad=-\ln[|1-\tan\theta\,\tan\Phi L|\,|1+\tan\theta\,\tan\Phi L|^{-1}]\end{aligned} \tag{46}$$

by using standard trigonometric identities. Now if

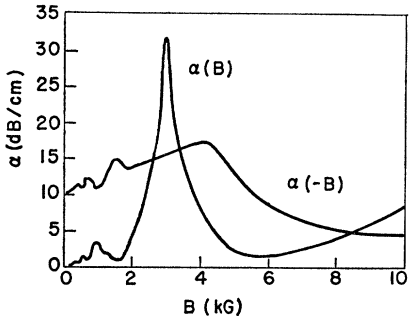

FIG. 6. Examples of $\alpha(\mathbf{B})$ and $\alpha(-\mathbf{B})$ at 92 Mc/sec. The zero of the $\alpha(-\mathbf{B})$ curve is shifted 10 dB/cm upward for clarity.

$-1<\tan\theta\,\tan\Phi L<1$, i.e., $\theta-\pi/2<\Phi L<\pi/2-\theta$,

$$\tan\Phi L=\frac{1-\exp\{[\alpha(\mathbf{B})-\alpha(-\mathbf{B})]L\}}{\tan\theta\{1+\exp\{[\alpha(\mathbf{B})-\alpha(-\mathbf{B})]L\}\}}. \quad (47)$$

If $\pi/2-\theta<\Phi L<\pi/2$ or $-\pi/2<\Phi L<\theta-\pi/2$, then we obtain

$$\tan\Phi L=\frac{1+\exp\{[\alpha(\mathbf{B})-\alpha(-\mathbf{B})]L\}}{\tan\theta\{1-\exp\{[\alpha(\mathbf{B})-\alpha(-\mathbf{B})]L\}\}}. \quad (48)$$

If $|\Phi L|>\pi/2$ one merely computes ΦL from Eq. (48) and then takes the true value as $\pi-\Phi L$ or $-\pi-\Phi L$. Thus, using Eqs. (47) and (48) we may find the rotation from the two measured curves $\alpha(\mathbf{B})$ and $\alpha(-\mathbf{B})$. By adding the Eqs. (45) we find $A(B)$:

$$A(B)=[\alpha(\mathbf{B})+\alpha(-\mathbf{B})]/2 + (1/2L)\ln|\cos^2\Phi L-\tan^2\theta\sin^2\Phi L|. \quad (49)$$

$\alpha(\mathbf{B})$ and $\alpha(-\mathbf{B})$ are automatically punched on paper tape and the two sets of data then interpolated on the CDC 1604 at certain values of B by fitting a cubic equation through six data points, three points on each side of the interpolated point. Then $\Phi(B)$ and $A(B)$ are computed according to the above formulas and automatically plotted versus B and ν/B, where ν is now the frequency of sound. The results of the measurements and calculations are given in the next section.

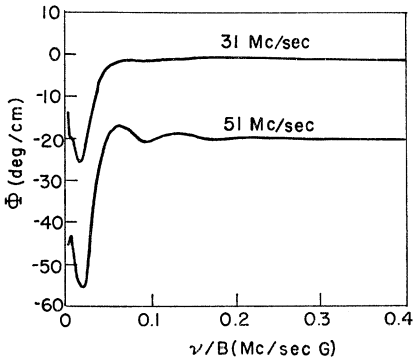

FIG. 7. Rotation of the plane of polarization of shear waves propagated along [001] in copper versus ν/B. The zero of the 51 Mc/sec curve is shifted down 20 deg/cm for clarity.

V. EXPERIMENTAL RESULTS

Representative examples of $\alpha(\mathbf{B})$ and $\alpha(-\mathbf{B})$ are shown in Fig. 6. The effect of the rotation of the plane of polarization is evident in these graphs. The sharp peak in $\alpha(\mathbf{B})$ is caused by the plane of polarization having rotated to a direction perpendicular to the sensitive direction of the receiving transducer.

Plots of Φ versus ν/B are shown in Figs. 7–9. Plots of A versus B are shown in Fig. 10. Since the periodicity of the A versus ν/B graphs is evident only for frequencies of 92 and 110 Mc/sec, only these are shown in Fig. 11. It can be seen, however, that the graphs of Φ versus ν/B are quasiperiodic even at 51 Mc/sec.

A note of explanation concerning the graphs shown is due. The rotation graphs were computed first from the data using Eq. (47). The field value at which the dashed line appears is that at which the plane of polarization has rotated to 90° from the sensitive direction of the receiving transducer. From that point on, Eq. (48) should be used to compute Φ. If one does this, however, it is found that the resulting curve does not join the curve computed from Eq. (47) at the field point in question. This discrepancy is ascribed to the fact that the acoustic wave is no longer plane polarized, but that it is elliptically polarized. It was pointed out in Sec. IV that near the point where $\theta-\Phi L=\pm\pi/2$ we expect Eqs. (47) and (48) to break down because, in deriving them, the effect of ellipticity was ignored. No matter how small the ellipticity is, when the major axis of the polarization is 90° from the direction of polarization of the receiving transducer, the minor axis gives the entire contribution to the signal.

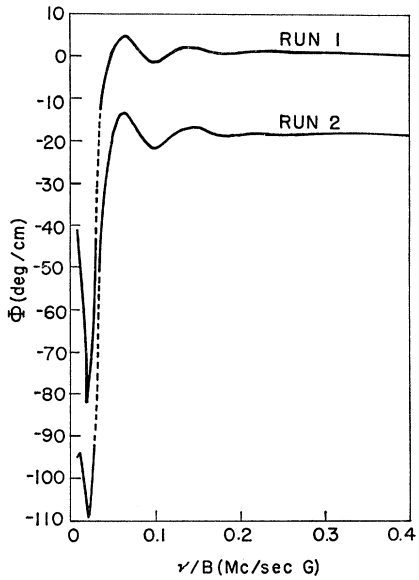

FIG. 8. Rotation of the plane of polarization of shear waves propagated along [001] in copper versus ν/B for two runs at 70.8 Mc/sec. This graph indicates the reproducibility of the data for two different transducer bonds. The zero of the lower curve is shifted downward 20 deg/cm for clarity.

Therefore, in the presentation of the curves, the solid lines are computed from Eqs. (47) and (48) [if Eq. (48) is required], and the breaks in the curves are indicated by a dashed line.

A certain amount of rotation, attenuation, and ellipticity is introduced at the interface between the bonding material and the sample. This is caused by the mismatch of the acoustic impedances of the two materials and is a function of the magnetic field and the bond thickness. The effects of these bond properties on the absolute values of the attenuation are difficult to isolate, but they appear to have no effect on the positions of the peaks, as evidenced by the fact that the peaks always appear at the same field values, even when different bonds are used.

The behavior of the plots follows the description in Sec. II. The Φ versus ν/B curves have twice the period of the A versus ν/B curves as the theory predicts. An absorption edge can be seen in the graphs of A versus B but it is not of the type discussed by Kjeldaas.[1] It is modified in the manner predicted by Kaner, Peschanskii, and Privorotskii.[17] That is, the absorption edge is preceded by a peak in the attenuation, since the edge is caused by electrons lying within a band on the Fermi surface which approaches some intermediate plane $k_1<k_z^{\max}$ on the surface as the absorption edge field is approached. Under these conditions, the absorption edge itself has no simple relationship to the dimensions of the Fermi surface as in the free-electron model. Nevertheless, there is a direct relationship between the shape of the attenuation curve and the properties of the Fermi surface, the interpretation of which is given in Sec. VI.

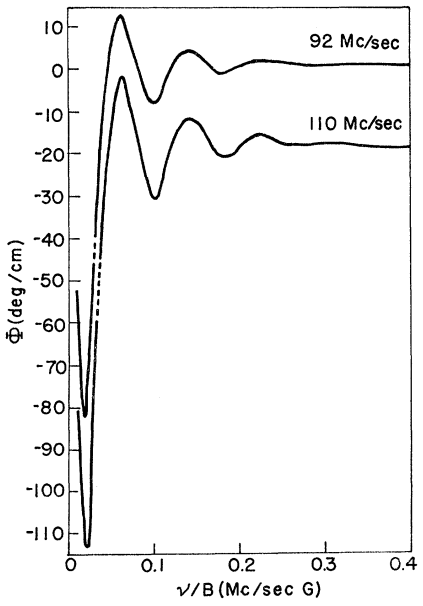

FIG. 9. Rotation of the plane of polarization of shear waves propagated along [001] in copper versus ν/B. The zero of the lower curve is shifted downward 20 deg/cm for clarity.

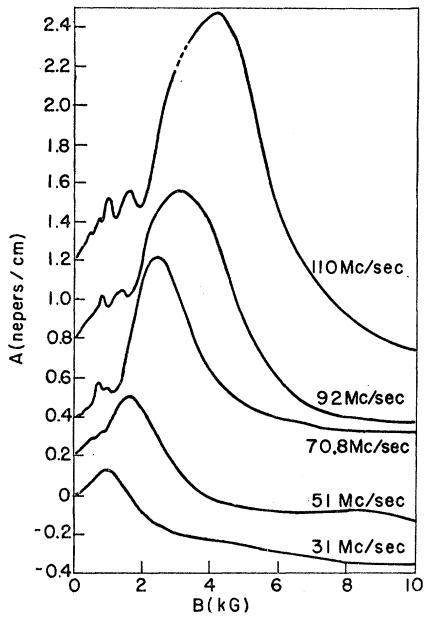

FIG. 10. Relative attenuation of shear waves propagated along [001] in copper versus magnetic field for several frequencies. The zeroes of all except the 31-Mc/sec curve have been shifted for clarity of presentation.

As was mentioned in Sec. II, a measurement of $\Delta_0=3^{-1/2}(\omega_{c0}\tau)^{-1}$ would determine the quantity $\omega_{c0}\tau$, where ω_{c0} is the electron cyclotron frequency at the point halfway between the fundamental peaks in the rotation and attenuation curves. We recall from Sec. II that the peaks of the attenuation curve are shifted by $+\Delta_0$ from the condition $|q\bar{v}_z/\omega_c|=(2n+1)$, whereas the

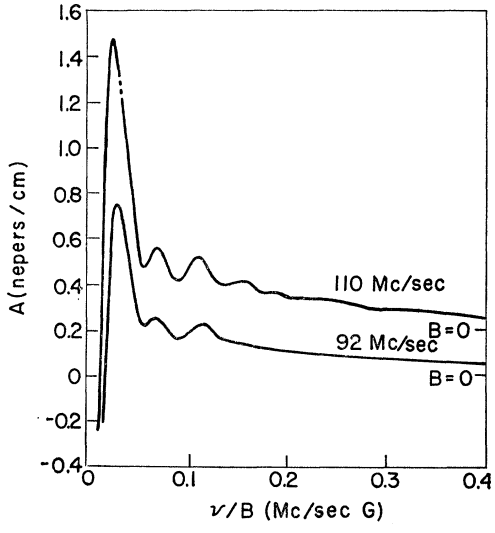

FIG. 11. Relative attenuation of shear waves propagating along [001] in copper versus ν/B for 92 and 110 Mc/sec. The zero of the 110 Mc/sec curve is shifted downward 0.2 neper/cm for clarity.

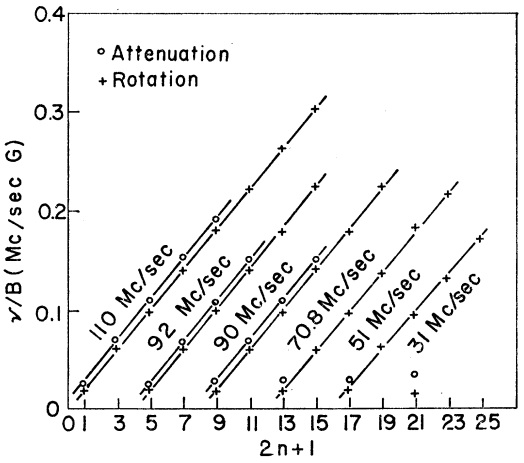

FIG. 12. ν/B versus $2n+1$ for successive peaks in the attenuation curves and for successive peaks and valleys in the rotation curves for several frequencies. All but the 110 Mc/sec curve are shifted successively to the right for clarity of presentation.

peaks of the rotation curve are shifted by $-\Delta_0$ from this same condition. The quantity Δ_0 is given, therefore, by one-half the vertical distance between the lines plotted for the attenuation and rotation peaks in Fig. 12 divided by the slope of the lines. Figure 12 is a graph of values of ν/B versus $(2n+1)$ for the successive peaks in the attenuation curves and for successive peaks and valleys in the rotation curves. Successive peaks and valleys were plotted in the case of the rotation curves because, as was pointed out in Sec. II, the selection rule $|q\bar{v}_z/\omega_c| = (2n+1)$ corresponds to peaks in the attenuation curve and valleys in the rotation curve for even values of n, but it corresponds to peaks in both curves for odd values of n. It should be noted that the intercept of the rotation plot in Fig. 12 should be $-\Delta_0$, whereas it appears to go through the origin. The reason for this is not known. Perhaps the numerator of Eq. (27) gives rise to an additional phase shift over that which we have considered.

To obtain Δ_0 from the data, one merely requires the vertical distance between the lines in Fig. 12 and the slope of the lines. For the frequencies where there was only one peak (valley) to plot so that the slope could not be determined, the slope of the other lines was used. The slope of the lines is 0.0201 ± 0.0005 Mc/sec G. Table I summarizes the results obtained for the values of Δ_0.

TABLE I. Summary of data relating to the phase of the attenuation and rotation peaks in Fig. 12. B_0 is the value of B at the point halfway between the fundamental peaks in the attenuation and rotation. The last column is computed from B_0 and $\omega_{c0}\tau$ by assuming the cyclotron mass to be that of a free electron.

Frequency (Mc/sec)	Average Δ_0	Number of points in average	$\omega_{c0}\tau$	ν/B_0 (Mc/G)	τ using free-electron ω_c (10^{-11} sec)
110	0.23	5	2.5	0.0250	3.2
92	0.25	4	2.3	0.0255	3.7
90	0.23	4	2.5	0.0250	3.9
70.8	0.28	2	2.1	0.0245	4.2
51	0.30	2	1.9	0.0255	5.6
31	0.45	1	1.3	0.0250	6.0
30.8	0.45	1	1.3	0.0250	6.0

The values of $\omega_{c0}\tau$ in Table I should be considered reliable only to an order of magnitude. In determining Δ_0 it is necessary to subtract two small and nearly equal values of ν/B. The values of ν/B are known to better than 1%, but the position of a given peak with respect to ν/B is only known to about 2% in this experiment. Upon performing the necessary subtraction to find Δ_0, the error in Δ_0 is about 20%. In order to determine Δ_0, and hence $\omega_{c0}\tau$, to within $\pm4\%$, it would be necessary to be able to determine the position of a given peak to within $\pm0.5\%$ with respect to ν/B. The above values of τ, however, are of the same order of magnitude as those found by Deaton and Gavenda[21] in a study of the limiting attenuation at high-field values on the same copper sample.

We note that the peaks in the attenuation and rotation curves do not scale exactly with frequency. This is because the attenuation peaks are shifted by $+\Delta_0$ and the rotation peaks and valleys are shifted by $-\Delta_0$ from the condition $|q\bar{v}_z/\omega_c| = (2n+1)$. It can be seen from Table I, however, that the value of ν/B midway between the attenuation peaks and rotation peaks (or valleys) does scale reasonably well with frequency, as it should.

In principle one would find the value of $|m_c\bar{v}_z|$ at the plane of the Fermi surface where $(m_c\bar{v}_z)' = 0$. One would simply use the equations

$$|m_c\bar{v}_z| = eB(2n+1+\Delta_0)/cq$$

and

$$|m_c\bar{v}_z| = eB(2n+1-\Delta_0)/cq$$

for the attenuation and rotation, respectively. In reality, as we shall see in Sec. VI, the result will be an average value of $|m_c\bar{v}_z|$ weighted over several sections of the Fermi surface according to the strength of the interaction between the sound wave and electrons on different portions of the Fermi surface. The value of $|m_c\bar{v}_z|$ which can be measured is given by

$$|m_c\bar{v}_z| = ec_s[2\pi c\Delta(\nu/B)]^{-1},$$

where $\Delta(\nu/B)$ is the period of the oscillations given by the slope of the lines in Fig. 12. The values we obtain is $|m_c\bar{v}_z| = 0.381\pm0.009\times10^{-19}$ g cm/sec, using $\Delta(\nu/B) = 0.0201\pm0.0005$ Mc/G and $c_s = 3.00\times10^5$ cm/sec.

In Fig. 13 a plot of Φ versus B at 92 Mc/sec is shown for comparison with the free-electron results shown in Fig. 3. The general shape is similar, but there are important differences. The experimental results show the higher harmonic oscillations in Φ at magnetic field

[21] B. C. Deaton and J. D. Gavenda, Phys. Rev. **129**, 1990 (1963).

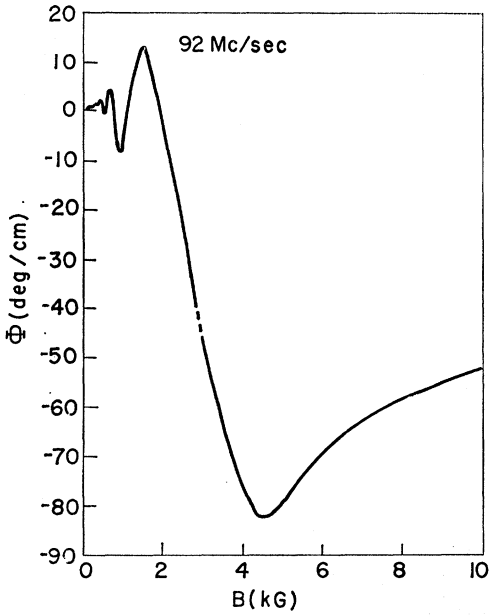

FIG. 13. Rotation of the plane of polarization of 92 Mc/sec shear waves propagated along [001] in copper versus magnetic field. Compare with the free-electron result in Fig. 3.

values below that for the fundamental oscillation. These oscillations are caused by the fourfold symmetry of the copper Fermi surface in the [001] direction. We also note that the fundamental oscillation occurs at a field value somewhat more than one-fourth of that for the free-electron model. As we shall see in Sec. VI, this is because the absorption edge is caused by a section of the Fermi surface where $m_c\bar{v}_z$ is only a fraction of that for the free-electron case.

VI. INTERPRETATION OF RESULTS

The results of the preceding section can be interpreted in terms of the Fermi surface of copper. Harrison[22] has shown that

$$m_c\bar{v}_z=-(\hbar/2\pi)(\partial S/\partial k_z), \tag{50}$$

where S is the cross-sectional area of the Fermi surface perpendicular to the direction of **B**. However, from the resonance condition [Eq. (26)] we find that

$$-2\pi\nu m_c\bar{v}_z c/ec_sB=4n\pm1$$

for electrons making the major contribution to the attenuation. If we ignore the subharmonic resonances for the moment (i.e., set $n=0$) we have

$$-m_c\bar{v}_z=ec_sB/2\pi\nu c, \tag{51}$$

and therefore it follows that

$$B(k_z)=(h\nu c/ec_s)(\partial S/\partial k_z). \tag{52}$$

Roaf[8] has published an empirical equation for the Fermi surface of copper. The equation was deduced from de Haas–van Alphen and anomalous-skin-effect data. Using Roaf's equation and Eq. (52) we may find B as a function of k_z. The attenuation is expected to be proportional to the number of electrons on the bands of the Fermi surface which contribute to Eq. (29). It then follows, as shown in Appendix B, that the attenuation $A(k_z)$ caused by a band of electrons of width Δk_z centered on k_z is given approximately by

$$A(k_z)\propto m_c(k_z)\Delta k_z. \tag{53}$$

If we assume that Roaf's equation is valid for energies other than the Fermi energy, we may use it to compute $m_c(k_z)$. Then, by eliminating k_z between Eqs. (52) and (53), we can plot A versus B. Since $m_c(k_z)$ serves only as a weighting factor, we only need to know its variation over the surface. The relative values computed from Roaf's equation agree rather well with the cyclotron resonance data of Koch, Stradling, and Kip.[23]

Figure 14 shows the central cross section of the copper Fermi surface in the (110) plane according to Roaf. Figure 15 shows a plot of the cross-sectional area S versus k_z in the [001] direction, Fig. 16 shows a plot of $|\partial S/\partial k_z|$ versus k_z, and Fig. 17 shows a graph of m_c/m_B versus k_z for k_z along the [001] direction. In calculating the attenuation caused by a band at a given value of k_z, Δk_z was taken to be 0.025×10^8 cm^{-1}. This was equivalent to taking 53 bands to cover half of the Fermi surface.

In Fig. 14 we see that from $k_z=0$ to approximately $k_z=0.60\times10^8$ cm^{-1} the orbits are electron orbits. From $k_z=0.60\times10^8$ cm^{-1} to 0.96×10^8 cm^{-1} the orbits are hole orbits which form the so-called "rosette" through four Brillouin zones. From $k_z=0.96\times10^8$ cm^{-1} to the limiting point of the Fermi surface at $k_z=1.33\times10^8$ cm^{-1} the orbits are again electron orbits.

Recalling the discussion in Sec. II, where it was shown that the peaks in the attenuation and rotation curves are caused by those portions of the Fermi surface where $(m_c\bar{v}_z)'\cong0$, we see from Fig. 16 that the section of the copper Fermi surface most likely to cause the peaks is the section centered around the point $k_z=0.45\times10^8$ cm^{-1}. One may also see from Fig. 16 that the

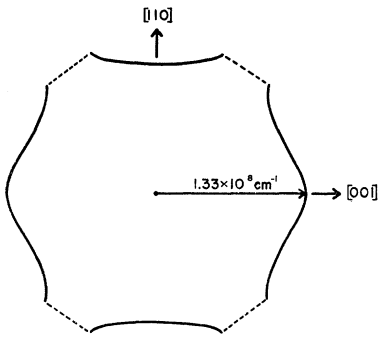

FIG. 14. Central cross section of the copper Fermi surface in the (110) plane according to Roaf. The dashed lines represent the intersection of the Fermi surface with the Brillouin zone.

[22] W. A. Harrison, Phys. Rev. 118, 1190 (1960).

[23] J. F. Koch, R. A. Stradling, and A. F. Kip, Phys. Rev. 133, A240 (1964).

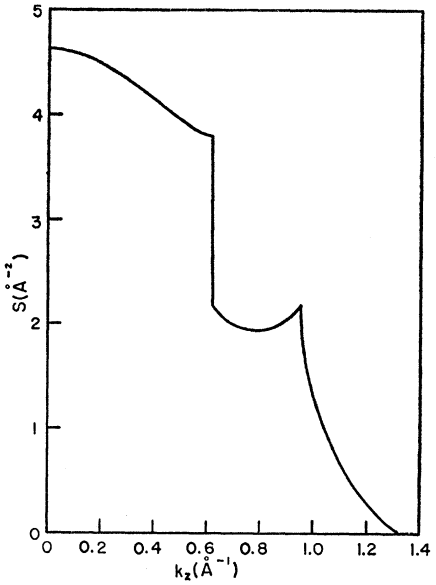

FIG. 15. Cross-sectional area of the Fermi surface of copper versus k_z for k_z in the [001] direction, according to Roaf.

quantity $b \equiv (q\bar{v}_z/\omega_c)''$ is negative for this portion of the surface since b is proportional to $(m_c\bar{v}_z)''$ and hence to $-(\partial S/\partial k_z)'$. There are, to be sure, other parts of the Fermi surface where $(m_c\bar{v}_z)'=0$, but this section covers the largest range in k_z and hence dominates the others because more electrons contribute to the attenuation. Numerical calculations indeed verify that the section of the Fermi surface from approximately $k_z=0.2\times10^8$ cm^{-1} to 0.58×10^8 cm^{-1} gives rise to most but not all of the attenuation at the peaks. The calculations were carried out numerically in the following manner.

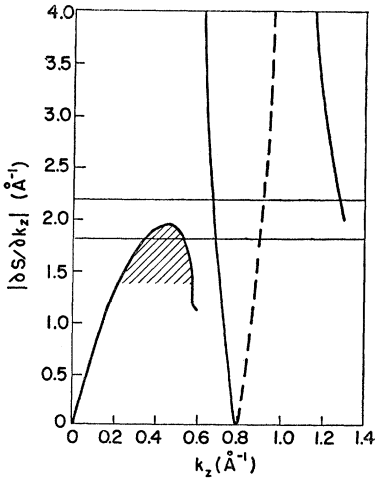

FIG. 16. $|\partial S/\partial k_z|$ for the Fermi surface of copper versus k_z for k_z in the [001] direction. The dashed line indicates where $\partial S/\partial k_z$ is positive, the solid where it is negative. The lines terminating at the top of the figure approach $k_z=0.60\times10^8$ cm^{-1} and $k_z=0.96\times10^8$ cm^{-1} asymptotically. The upper horizontal line represents the experimental value of $|\partial S/\partial k_z|$ measured from the slopes of the lines in Fig. 12. The lower horizontal line represents the value of $|\partial S/\partial k_z|$ calculated for B at the large peak in Fig. 18. The shaded area indicates that portion of the Fermi surface which gives the major contribution to the attenuation.

From Eq. (33) it can be seen that the half-width of the resonant denominator in terms of the quantity $q\bar{v}_z/\omega_c$ (see Appendix A) is $(\omega_c\tau)^{-1}$. In terms of the quantity $-(\partial S/\partial k_z)$ the half-width is [by use of Eq. (50)]

$$-(\partial S/\partial k_z)=2\pi m_c/q\hbar\tau. \tag{54}$$

Using $\tau=4.8\times10^{-11}$ sec (the average of the values in Table I), the free-electron mass for m_c, and the value of q appropriate to 110 Mc/sec we find the half-width in terms of $-(\partial S/\partial k_z)$ to be approximately 0.5×10^8 cm^{-1}. A value of $-(\partial S/\partial k_z)$ [corresponding to a value of B through Eq. (52)] is selected and electrons lying within a range of $\pm0.75\times10^8$ cm^{-1} on the ordinate of Fig. 16 are assumed to contribute to the attenuation. This region is then divided into three equal parts. Each of these parts defines a range over k_z on the abscissa. Then the area under the curve of m_c in Fig. 17 is found for each of the three regions of k_z. The area for the range closest to the resonance is weighted by 0.9, the next one by 0.65, and the last one by 0.4 in an attempt to approximate the actual character of the resonance denominator in Eq. (29). The resulting number is then plotted at the value of B corresponding to the central value of $-(\partial S/\partial k_z)$. This should be equivalent to a plot of A versus B. This plot is shown in Fig. 18 and compared with the experimental results at 110 Mc/sec. The calculated attenuation has been scaled so that the two curves coincide at the peak, but B is computed directly from Roaf's surface using Eq. (52). The lower horizontal line in Fig. 16 shows the value of $-(\partial S/\partial k_z)$ corresponding to the value of B for the fundamental absorption peak. It corresponds to a value of $m_c\bar{v}_z=0.284\times10^{-19}$ g cm/sec.

It can be seen that the general shape of the calculated curve is similar to the experimental one, although no

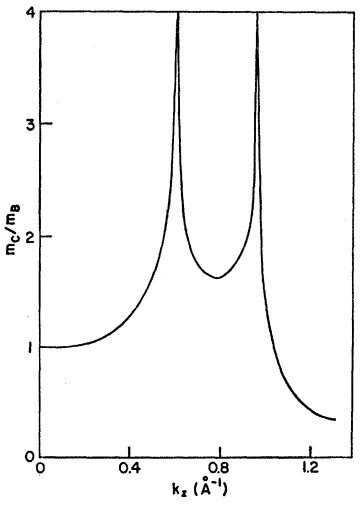

FIG. 17. Cyclotron mass for **B** along [001] normalized with respect to m_B, the cyclotron mass for $k_z=0$, assuming Roaf's equation valid near the Fermi surface as well as on it.

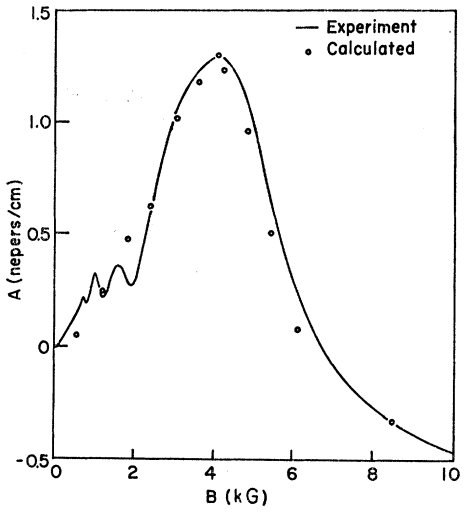

FIG. 18. Comparison of the experimental attenuation with the calculated attenuation at 110 Mc/sec. The ordinate of the calculated curve is chosen to fit at the main peak, but the abscissa is calculated from Roaf's surface using Eq. (52).

attempt was made to include the harmonic peaks in the calculated curve. The calculation shows that the character of the attenuation curve is caused almost entirely but not completely by the electrons on the Fermi surface with 0.2×10^8 cm$^{-1}<k_z<0.58\times10^8$ cm^{-1}. The neck orbits provide some background attenuation, and the orbits beyond the necks begin to come into play at fields corresponding to the fundamental absorption peak.

In Sec. V we found a value of $m_c\bar{v}_z=0.381\pm0.009\times10^{-19}$ g cm/sec from the periods of the oscillations in A and Φ. This should be the value of $m_c\bar{v}_z$ at the point where $(m_c\bar{v}_z)=0$, i.e., at the plane $k_z=0.45\times10^8$ cm^{-1}. By using Eq. (50) we find that this corresponds to $-(\partial S/\partial k_z)=2.28\pm0.06\times10^8$ cm^{-1}. This value is shown in Fig. 16 by the upper horizontal line. We note that it lies considerably above the value of 1.99×10^8 cm^{-1} expected from Roaf's surface.

The cause of the discrepancy between the value of $m_c\bar{v}_z$ obtained from the periods of the attenuation and rotation peaks and that obtained from the shape of the surface proposed by Roaf (which appears to explain the general form of the attenuation curve) can be found in Fig. 12. The straight lines drawn through the attenuation peaks do not pass through the origin. Instead, the first peak occurs at a considerably higher value of ν/B than would be obtained from the slope of the line through the points. That is, the first peak is observed at a lower value of magnetic field than one would expect from the period of the attenuation peaks.

The phase shift of the peaks results from the finite value of $1/\omega_c\tau$. A relatively large region of the Fermi surface contributes to the main resonance peak, and most of the contributing orbits have $m_c\bar{v}_z$ values less than that at $k_z=0.45\times10^8$ cm^{-1}. This region is indicated by the shaded area of Fig. 16. Thus the average obtained from an integral over all of the contributing orbits is less than the expected value.

For higher harmonic peaks a smaller band of orbits, with $m_c\bar{v}_z$ values closer to that at the peak, may contribute, so the slope of the lines connecting the peaks in Fig. 16 may be less than expected. This will result in a value of $m_c\bar{v}_z$ larger than the true value. It is also possible that the period may be affected by the fact that the a_n are functions of k_z, rather than constant as assumed in the derivation earlier.

The fact that the two different approaches yield values of $m_c\bar{v}_z$ on either side of that predicted from Roaf's surface is good evidence for the validity of that surface, at least near the plane $k_z=0.45\times10^8$ cm^{-1}.

VII. SUMMARY

The rotation of the plane of polarization of shear sound waves propagating parallel to an external magnetic field in copper has been measured. The rotation is periodic in ν/B. The attenuation peaks described by Kaner, Peschanskii, and Privorotskii[17] have been observed and they are also periodic in ν/B.

A real-metal theory based upon the fourfold symmetry of the copper Fermi surface has been presented along the lines suggested by Kotkin.[2] The results of this theory show that the attenuation has a period half that of the rotation and that the selection rule for the attenuation peaks is $q\bar{v}_z/\omega_c=2n+1+\Delta_0$, whereas for the rotation peaks it is $q\bar{v}_z/\omega_c=2n+1-\Delta_0$, odd values of n giving positive peaks and even giving negative peaks, where $\Delta_0=3^{-1/2}(\omega_{c0}\tau)^{-1}$. The experimental results are in general agreement with the theory but it is not possible to determine a precise value for Δ_0.

The fundamental attenuation peak was calculated numerically from the Fermi surface of copper deduced by Roaf[8] and compared with the experimental results at 110 Mc/sec. The principal features of the attenuation curve are accounted for by the calculation.

Finally, it has been demonstrated that one must be rather cautious about identifying an absorption edge with a radius of curvature of the Fermi surface at a certain point since the absorption edge may be caused, not by one point on the Fermi surface, but by a rather large portion of the surface.

ACKNOWLEDGMENTS

The authors gratefully acknowledge many helpful discussions with D. B. Doan concerning the computer programming and electronic equipment, and the use of his computer program for Roaf's equation.

Thanks also go to Dr. L. M. Falicov for suggesting the interpretation of this work in terms of Roaf's equation for the Fermi surface, to Dr. W. G. Chambers and Dr. P. R. Antoniewicz for helpful discussions, and to F. H. S. Chang and B. Yee for their help in many ways.

APPENDIX A

We wish to evaluate integrals of the type

$$R_n=\int_{-k_z\max}^{k_z\max}\frac{dk_z}{1+\tau^2[q\bar{v}_z-(2n+1)\omega_c]^2},$$

where we have assumed $\bar{v}_z>0$ near the point where $(q\bar{v}_z/\omega_c)'=0$. We assume only one such point over the range of integration but the result can easily be generalized. Let $\xi=(\omega_c\tau)^{-1}$ and $\theta=q\bar{v}_z/\omega_c$. We expand $\theta(k_z)$ about the stationary point $k_z=k_1$:

$$\theta(k_z)\cong\theta(k_1)+(b/2)(k_z-k_1)^2,$$

where $b\equiv(\partial^2\theta/\partial k_z^2)_{k_1}$, so that the denominator can be rewritten as

$$\tau^2[q\bar{v}_z-(2n+1)\omega_c]^2=\omega_c^2\tau^2[\theta(k_z)-(2_n+1)]^2$$
$$=[\mu_n+(b/2)(k_z-k_1)^2]^2/\xi^2,$$

where

$$\mu_n=\theta(k_1)-(2n+1). \tag{A1}$$

For $\omega_c\tau\gg1$ the integrand is a peaked function for $k_z\cong k_1$ and nearly zero elsewhere, so the range of integration may be taken to be from $-\infty$ to $+\infty$. Thus letting $x=(k_z-k_1)$ we have

$$R_n=\int_{-\infty}^{\infty}\frac{\xi^2dx}{\xi^2+(\mu_n+bx^2/2)^2}.$$

The roots of the denominator in the complex plane are

$$z=\pm[2(\pm i\xi-\mu_n)/b]^{1/2}.$$

We perform the standard integration in the upper half of the complex plane around the semicircle $R>|z|$ and then let $R\to\infty$. There are simple poles at z_1 and z_2 in the upper half-plane.

$$z_1=-(\operatorname{sgn}b)[(-\operatorname{sgn}b)2(i\xi+\mu_n)/|b|]^{1/2},$$
$$z_2=(\operatorname{sgn}b)[(\operatorname{sgn}b)2(i\xi-\mu_n)/|b|]^{1/2}.$$

The value of the integral is $2\pi i(K_1+K_2)$, where K_1 and K_2 are the residues at z_1 and z_2.

$$K_1=\xi/2i[-2|b|(i\xi+\mu_n)(\operatorname{sgn}b)]^{1/2},$$
$$K_2=\xi/2i[2|b|(i\xi-\mu_n)(\operatorname{sgn}b)]^{1/2}.$$

Thus we obtain

$$R_n=2\pi\xi|b|^{-1/2}M_1(b,\xi,\mu_n),$$

where

$$M_1(b,\xi,\mu_n)$$
$$=[(\xi^2+\mu_n^2)^{1/2}-\mu_n(\operatorname{sgn}b)]^{1/2}(\xi^2+\mu_n^2)^{-1/2}. \tag{A2}$$

The rotation integrals are of the form

$$I_n=\int_{-\infty}^{\infty}\frac{\xi(\mu_n+bx^2/2)dx}{\xi^2+(\mu_n+bx^2/2)^2}.$$

The poles are the same as in the previous integral, but the residues are different. They are

$$K_1=-\xi/2[-2|b|(i\xi+\mu_n)(\operatorname{sgn}b)]^{1/2},$$
$$K_2=\xi/2[2|b|(i\xi-\mu_n)(\operatorname{sgn}b)]^{1/2}.$$

The result for I_n is

$$I_n=2\pi\xi|b|^{-1/2}M_2(b,\xi,\mu_n),$$

where

$$M_2(b,\xi,\mu_n)$$
$$=[(\xi^2+\mu_n^2)^{1/2}+\mu_n(\operatorname{sgn}b)]^{1/2}(\xi^2+\mu_n^2)^{-1/2}. \tag{A3}$$

We note that the only difference between Eqs. (A2) and (A3) is the change of the sign of μ_n.

APPENDIX B

The attenuation caused by the electrons lying within a band of a given width centered on k_z is expected to be proportional to the number of electrons on the band, which in turn is proportional to the electron density of states on the band times its width, Δk_z.

The density of states per unit energy range on the Fermi surface is given by

$$N(\epsilon_F)=(8\pi^3n_0)^{-1}\int\int|\partial\epsilon/\partial k|^{-1}df, \tag{B1}$$

where df is the element of the Fermi surface and n_0 is the number of electrons/cm^3. However, $|\hbar v|=|\partial\epsilon/\partial k|$ and $df/|\hbar v|=(m_c/\hbar^2)dk_zd\phi$, so we have

$$N(\epsilon_F)=(h^2n_0)^{-1}\int m_cdk_z; \tag{B2}$$

therefore the number of electrons per unit energy range per cm^{-1} at the plane k_z is $m_c(k_z)/h^2n_0$. One thus expects the attenuation produced by a band of electrons at k_z to be given by the following expression:

$$A(k_z)\propto m_c(k_z)\Delta k_z. \tag{B3}$$